Final Report

on

SPC 97-4046

COMPUTATIONAL DAMAGE MODEL FOR LAMINATED COMPOSITE MATERIALS PHASE II.

Principal Investigator:

Prof.,Dr.Sc.(hab.) *N.N.Smirnov*

Investigators:

Prof.,Dr.Sc.(hab.) *A.B.Kiselev*
M.Sc. *V.F.Nikitin*
Dr. *V.M.Shevtsova*
Dr. *M.V.Yumashev*

MOSCOW-BRUSSELS - 1998

REPORT DOCUMENTATION PAGE

Form Approved OMB No. 0704-0188

1. AGENCY USE ONLY (Leave blank)	2. REPORT DATE	3. REPORT TYPE AND DATES COVERED
	1998	Final Report

4. TITLE AND SUBTITLE

Computational Damage Model for Laminated Composite Materials-Phase II

5. FUNDING NUMBERS

F6170897W0163

6. AUTHOR(S)

Prof. Nickolay Smirnov

7. PERFORMING ORGANIZATION NAME(S) AND ADDRESS(ES)

Moscow State University
Faculty of Mechanics and Mathematics
Moscow 119899
Russia

8. PERFORMING ORGANIZATION REPORT NUMBER

N/A

9. SPONSORING/MONITORING AGENCY NAME(S) AND ADDRESS(ES)

EOARD
PSC 802 BOX 14
FPO 09499-0200

10. SPONSORING/MONITORING AGENCY REPORT NUMBER

SPC 97-4046

11. SUPPLEMENTARY NOTES

12a. DISTRIBUTION/AVAILABILITY STATEMENT

Approved for public release; distribution is unlimited.

12b. DISTRIBUTION CODE

A

13. ABSTRACT (Maximum 200 words)

This report results from a contract tasking Moscow State University as follows: The contractor will develop a physical model describing delamination process. He will perform detailed models for damageable composite elements for 3-D, 2-D cases for thin shells, plates, rods, bars, as detailed in his proposal dated 22 March 97.

14. SUBJECT TERMS

Aircraft Subsystem; Hydrodynamic Ram Problem

15. NUMBER OF PAGES

38

16. PRICE CODE

N/A

17. SECURITY CLASSIFICATION OF REPORT	18. SECURITY CLASSIFICATION OF THIS PAGE	19, SECURITY CLASSIFICATION OF ABSTRACT	20. LIMITATION OF ABSTRACT
UNCLASSIFIED	UNCLASSIFIED	UNCLASSIFIED	UL

Contents

Summary

The present final Report contains final chapters 4, 5 and 6 describing the Computational Damage Model for Thermoviscoelastic Laminated Composite Materials. The detailed models for damageable composite elements for the general 3D case was described in [1], Chapters 1 and 2. The model was based on detailed physical description and developed kinetic equations for accumulations of damages in shear, tension and delamination. The model constants were distinguished that should be determined from the experiments.

The Chapter 3 [2] contained the description of the experimental procedure on twisting and tension of thin-walled tubular samples. The application of the damage model for 2D cases of deforming thin shells was developed. Some solutions were obtained within the frames of quasistatical approximation enabling to develop some of the damage constants for low rates of loading. Recommendations for developing constants by comparing experimental and theoretical results were worked out.

The present report contains the derivation of the model equations for quasidynamical problems on twisting and tension of tubular thin shells (Chapter 4). The solutions of the problem are obtained for different rates of loading (Chapter 5). Based on the obtained solutions for dynamical behavior of parameters under different rates of loading (twisting and tension) detailed recommendations are worked out for the test procedures wich need to be performed to develop the constants for the model of damageable laminated composite materials.

The Chapter 6 contains the developed mathematical methods to model numerically the behavior of material and its further dynamical deforming after accumulation of damages leads to destruction of material in the damaged zone.

Chapter 4

Quasidynamical problems of deforming and breakup of thin-walled cylindrical tubular two-phase laminated composite samples

We regard the classical problems of quasidynamical twisting or tension of a thin-walled tubular sample. The length of the sample is denoted L, the radius (external) a, the thickness of the walls h ($h/a \ll 1$, $a/L \ll 1$). Let the sample be loaded monotonously by the growing rotating moment $M = M(t)$ ($\dot{M}(t) > 0$) applied to the end points of the sample along the z-axis, or by axial tensile forces $F = F(t)$ ($\dot{F}(t) > 0$) (Fig. 4.1).

In the very beginning ($t = t_0$) there are no stresses and strains in the sample and its temperature is uniform ($T = T_0$). Let the time of loading until breakup be much larger than the characteristic time of elastic wave traveling along the sample but much less than the characteristic time of heat propagation along the sample due to thermal conductivity. Then the problem could be regarded within the frames of quasidynamical approximation. In fact the term "quasidynamical" means that we apply a quasistatical approximation to mechanical processes and adiabatic approximation to the thermal processes.

4.1 Twisting of a thin-walled tubular sample

In case of pure twisting of a sample $F(t) \equiv 0$ only one component of the stresses tensor (shear stress $\sigma_{\theta z}$) differes from zero:

$$\sigma_{\theta z}(t) = \frac{M(t)}{2\pi a^2 h}.$$

Let $\sigma_{\theta z}(t) = f \cdot t, \quad f = \text{const} > 0.$

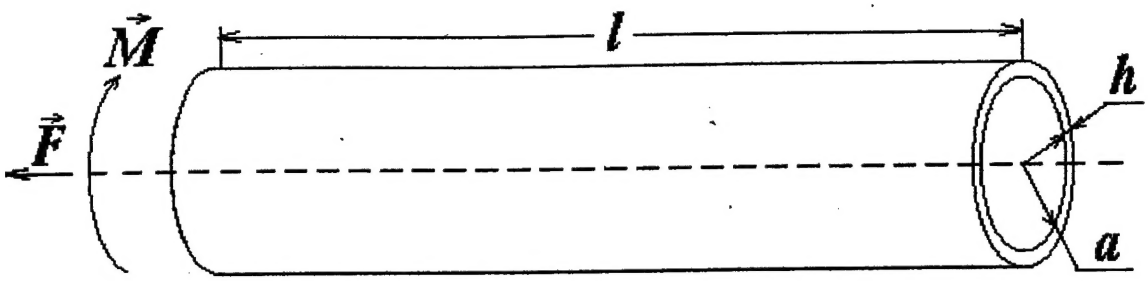

fig. 4.1.

Then the system of constitutive equations for the problem will take the form:

$$(C_{22}-C_{23})\varepsilon^e_{\theta z}+2AC\log(1-\alpha)\frac{\varepsilon^e_{\theta z}}{e^e_u}=ft,$$

$$\dot\varepsilon_{\theta z}-\dot\varepsilon^e_{\theta z}=(\alpha_{22}-\alpha_{23})ft+\beta_2^-B_-\Delta_{\theta z}+\frac{4D\Lambda_\Delta}{1-\alpha}\log(1-\omega_\Delta)\frac{\beta_2^-\Delta_{\theta z}}{\Delta},$$

$$\dot\varepsilon^e_{zz}=\dot\varepsilon^e_{\theta\theta}=-\beta_2^+B_+(\Delta_+-\theta(T-T_0))-\frac{D\Lambda_\Delta}{2(1-\alpha)}\log(1-\omega_\Delta)\frac{\beta_2^+\Delta_+}{\Delta},$$

$$\dot\varepsilon^e_{rr}=-\beta_1^+B_+(\Delta_+-\theta(T-T_0))-\frac{D\Lambda_\Delta}{2(1-\alpha)}\log(1-\omega_\Delta)\frac{\beta_1^+\Delta_+}{\Delta},$$

$$\dot\Delta_+=-\gamma B_+(\Delta_+-\theta(T-T_0))-\frac{\gamma D\Lambda_\Delta}{2(1-\alpha)}\log(1-\omega_\Delta)\frac{\Delta_+}{\Delta},$$

$$\dot\Delta_{\theta z}=-2\beta_2^-ft-3\gamma B_-\Delta_{\theta z}-\frac{12\gamma D\Lambda_\Delta}{1-\alpha}\log(1-\omega_\Delta)\frac{\Delta_{\theta z}}{\Delta},$$

$$\dot\alpha=C\left(\frac{e^e_u}{1-\alpha}-\varepsilon^*_\tau\right)H\left(\frac{e^e_u}{1-\alpha}-\varepsilon^*_\tau\right),$$

$$\dot\omega_\Delta=D\left(\frac{\Delta}{(1-\alpha)(1-\omega_\Delta)}-\Delta_*\right)H\left(\frac{\Delta}{(1-\alpha)(1-\omega_\Delta)}-\Delta_*\right)$$

$$T\dot\eta=2ft(\dot\varepsilon_{\theta z}-\dot\varepsilon^e_{\theta z})-q_+\dot\Delta_+-q_{\theta z}\dot\Delta_{\theta z}+A\dot\alpha^2+\Lambda_\Delta\dot\omega_\Delta^2,$$

$$T=T_0-d_1\varepsilon^e_{rr}-2d_2\varepsilon^e_{zz}+P(\eta-B_+\theta\Delta_+), \tag{4.1}$$

where:

$$\Delta=\sqrt{\frac12\Delta_+^2+\Delta^2_{\theta z}},\qquad e^e_u=\sqrt{\frac23(\varepsilon^e_{zz}-\varepsilon^e_{rr})^2+2(\varepsilon^e_{\theta z})^2},$$

$$q_+=B_+(\Delta_+-\theta(T-T_0))+\frac{D\Lambda_\Delta}{2(1-\alpha)}\log(1-\omega_\Delta)\frac{\Delta_+}{\Delta},$$

$$q_{\theta z}=\frac12B_-\Delta_{\theta z}+\frac{2D\Lambda_\Delta}{1-\alpha}\log(1-\omega_\Delta)\frac{\Delta_{\theta z}}{\Delta}.$$

The constants used in (4.1) have the following form [2]:

$$C_{22}-C_{23}=2\langle\mu\rangle,\quad \alpha_{22}-\alpha_{23}=\frac{1}{2\langle\mu\rangle^2}\left\langle\frac{\mu}{\tau}\right\rangle,$$

$$\beta_1^+=\frac12\left(\frac{\Lambda_2}{\tau_2}-\frac{\Lambda_1}{\tau_1}\right),\quad \beta_2^+=\frac{1}{12\langle\hat E\rangle}\left(\frac{\hat E_1}{\mu_1\tau_1}-\frac{\hat E_2}{\mu_2\tau_2}\right),\quad \beta_2^-=\frac{1}{4\langle\mu\rangle}\left(\frac{1}{\tau_1}-\frac{1}{\tau_2}\right),$$

$$B_+=\frac{c(1-c)\hat E_1\hat E_2}{\langle\hat E\rangle},\quad B_-=\frac{c(1-c)\mu_1\mu_2}{\langle\mu\rangle},\quad \theta=\frac{\alpha_v^{(1)}-\alpha_v^{(2)}}{3},$$

$$\gamma = \frac{1}{12}\left(\frac{1}{c\mu_1\tau_1} + \frac{1}{(1-c)\mu_2\tau_2}\right),$$

$$\Lambda_\alpha = \frac{\hat{E}_\alpha}{3\mu_\alpha\left\langle\hat{E}\right\rangle}\left\langle\frac{\hat{\lambda}}{\hat{\lambda}+2\mu}\right\rangle + \frac{2}{3(\hat{\lambda}_\alpha+2\mu_\alpha)}, \quad \hat{E}_\alpha = \frac{\mu_\alpha(3\hat{\lambda}_\alpha+3\mu_\alpha)}{\hat{\lambda}_\alpha+2\mu_\alpha},$$

$$\hat{\lambda}_\alpha = \lambda_\alpha - \frac{(K_\alpha\alpha_v^{(\alpha)})^2}{c_\varepsilon^{(\alpha)}}T_0, \qquad (\alpha = 1,2) \tag{4.2}$$

where $\hat{E}_\alpha$ – isothermic Young modulus, $\hat{\lambda}_\alpha$ – isothermic Lamè coefficient. The physical meaning of all the constants was discussed in details in [1,2].

4.2 Tension of a thin-walled tubular sample

In case of pure tension of the sample ($M(t) \equiv 0$) only one component of stress tension σ_{zz} differes from zero:

$$\sigma_{zz}(t) = \frac{F(t)}{2\pi ah}.$$

Let $\sigma_{zz}(t) = f \cdot t$, $f = \text{const} > 0$.

Then the governing system of equations will have the following form:

$$C_{12}\varepsilon_{rr}^e + C_{22}\varepsilon_{zz}^e + C_{23}\varepsilon_{\theta\theta}^e - d_2(\eta - B_+\theta\Delta_+) + \Lambda\Omega\log(1-\omega) + \frac{AC}{3(1-\omega)}\log(1-\alpha)\frac{2\varepsilon_{zz}^e - \varepsilon_{rr}^e - \varepsilon_{\theta\theta}^e}{e_u^e} = ft,$$

$$\dot{\varepsilon}_{zz} - \dot{\varepsilon}_{zz}^e = \alpha_{22}ft + \beta_2^+B_+(\Delta_+ - \theta(T-T_0)) + \beta_2^-B_-\Delta_- + \frac{D\Lambda_\Delta}{2(1-\omega)(1-\alpha)}\log(1-\omega_\Delta)\frac{\beta_2^+\Delta_+ + \beta_2^-\Delta_-}{\Delta},$$

$$\dot{\varepsilon}_{rr}^e = -\alpha_{12}ft - \beta_1^+B_+(\Delta_+ - \theta(T-T_0)) - \frac{D\Lambda_\Delta}{2(1-\omega)(1-\alpha)}\log(1-\omega_\Delta)\frac{\beta_1^+\Delta_+}{\Delta},$$

$$\dot{\varepsilon}_{\theta\theta}^e = -\alpha_{23}ft - \beta_2^+B_+(\Delta_+ - \theta(T-T_0)) + \beta_2^-B_-\Delta_- - \frac{D\Lambda_\Delta}{2(1-\omega)(1-\alpha)}\log(1-\omega_\Delta)\frac{\beta_2^+\Delta_+ - \beta_2^-\Delta_-}{\Delta},$$

$$\dot{\Delta}_+ = -\beta_2^+ft - \gamma B_+(\Delta_+ - \theta(T-T_0)) - \frac{\gamma D\Lambda_\Delta}{2(1-\omega)(1-\alpha)}\log(1-\omega_\Delta)\frac{\Delta_+}{\Delta},$$

$$\dot{\Delta}_- = -\beta_2^-ft - 3\gamma B_-\Delta_- - \frac{3\gamma D\Lambda_\Delta}{2(1-\omega)(1-\alpha)}\log(1-\omega_\Delta)\frac{\Delta_-}{\Delta},$$

$$\dot{\omega} = \Omega\left(\frac{\varepsilon^e_{zz}+\varepsilon^e_{rr}+\varepsilon^e_{\theta\theta}}{1-\omega}-\varepsilon_*\right)H\left(\frac{\varepsilon^e_{zz}+\varepsilon^e_{rr}+\varepsilon^e_{\theta\theta}}{1-\omega}-\varepsilon_*\right),$$

$$\dot{\alpha} = C\left(\frac{e^e_u}{(1-\omega)(1-\alpha)}-\varepsilon^*_\tau\right)H\left(\frac{e^e_u}{(1-\omega)(1-\alpha)}-\varepsilon^*_\tau\right),$$

$$\dot{\omega}_\Delta = D\left(\frac{\Delta}{(1-\omega)(1-\alpha)(1-\omega_\Delta)}-\Delta_*\right)H\left(\frac{\Delta}{(1-\omega)(1-\alpha)(1-\omega_\Delta)}-\Delta_*\right),$$

$$T\dot{\eta} = ft(\dot{\varepsilon}_{zz}-\dot{\varepsilon}^e_{zz}) - q_+\dot{\Delta}_+ - q_-\dot{\Delta}_- + \Lambda\dot{\omega}^2 + A\dot{\alpha}^2 + \Lambda_\Delta\dot{\omega}^2_\Delta,$$

$$T = T_0 - d_1\varepsilon^e_{rr} - d_2(\varepsilon^e_{zz}+\varepsilon^e_{\theta\theta}) + P(\eta - B_+\theta\Delta_+), \tag{4.3}$$

where:

$$\Delta = \sqrt{\frac{1}{2}(\Delta_+^2+\Delta_-^2)}, \qquad e^e_u = \sqrt{\frac{1}{3}[(\varepsilon^e_{zz}-\varepsilon^e_{rr})^2+(\varepsilon^e_{zz}-\varepsilon^e_{\theta\theta})^2+(\varepsilon^e_{rr}-\varepsilon^e_{\theta\theta})^2]},$$

$$q_+ = B_+(\Delta_+ - \theta(T-T_0)) + \frac{D\Lambda_\Delta}{2(1-\omega)(1-\alpha)}\log(1-\omega_\Delta)\frac{\Delta_+}{\Delta},$$

$$q_- = B_-\Delta_- + \frac{D\Lambda_\Delta}{2(1-\omega)(1-\alpha)}\log(1-\omega_\Delta)\frac{\Delta_-}{\Delta}.$$

The constants in (4.3) that have not been described in (4.2) are the following:

$$P = \left\langle p^{-1}\right\rangle^{-1} - c(1-c)\frac{(\pi_2'-\pi_1')^2}{\tilde{\lambda}'+2\tilde{\mu}}; \quad \lambda'_\alpha = \lambda_\alpha - \frac{\tilde{\pi}}{\tilde{p}}\pi_\alpha, \quad \pi'_\alpha = \pi_\alpha - \frac{\tilde{\pi}}{\tilde{p}}p_\alpha,$$

$$p_\alpha = \frac{T_0}{c^{(\alpha)}_\varepsilon}, \quad \pi_\alpha = \frac{K_\alpha\alpha^{(\alpha)}_v}{c^{(\alpha)}_\varepsilon}T_0 \quad (\alpha=1,2);$$

$$C_{12} = \left\langle\frac{\lambda'}{\lambda'+2\mu}\right\rangle\left\langle\frac{1}{\lambda'+2\mu}\right\rangle^{-1} + \frac{\tilde{\pi}}{\tilde{p}}\left\langle\pi^{-1}\right\rangle^{-1};$$

$$C_{22} = \langle\lambda'+2\mu\rangle - c(1-c)\frac{(\lambda_2'-\lambda_1')^2}{\tilde{\lambda}'+2\tilde{\mu}} + \frac{\tilde{\pi}}{\tilde{p}}\left\langle\pi^{-1}\right\rangle^{-1}, \quad C_{23} = C_{22} - 2\langle\mu\rangle,$$

$$d_1 = \left\langle\frac{\pi}{p}\right\rangle\left\langle p^{-1}\right\rangle^{-1} - c(1-c)\frac{(\lambda_2'-\lambda_1'+2\mu_2-2\mu_1)((\pi_2'-\pi_1')}{\tilde{\lambda}'+2\tilde{\mu}},$$

$$d_2 = \left\langle\frac{\pi}{p}\right\rangle\left\langle p^{-1}\right\rangle^{-1} - c(1-c)\frac{(\lambda_2'-\lambda_1')(\pi_2'-\pi_1')}{\tilde{\lambda}'+2\tilde{\mu}},$$

$$\alpha_{12} = -\frac{1}{2\left\langle\hat{E}\right\rangle}\left\langle\frac{\hat{E}\Lambda}{\tau}\right\rangle,$$

$$\alpha_{22} = \frac{1}{12\left\langle\hat{E}\right\rangle^2}\left\langle\frac{\hat{E}^2}{\mu\tau}\right\rangle + \frac{1}{4\langle\mu\rangle^2}\left\langle\frac{\mu}{\tau}\right\rangle, \quad \alpha_{23} = \frac{1}{12\left\langle\hat{E}\right\rangle^2}\left\langle\frac{\hat{E}^2}{\mu\tau}\right\rangle - \frac{1}{4\langle\mu\rangle^2}\left\langle\frac{\mu}{\tau}\right\rangle.$$

Chapter 5

Dynamical behavior of governing parameters in deforming and breakup of thin-walled two-phase cylindrical tubular composite samples

The present chapter contains the results of numerical investigations of the damage parameters behavior for the model laminated composite material in possible experiments on twisting and tension of tubular samples for different rates of loading. Since the damage parameters cannot be measured directly in the experiment the data on the behavior of strains and temperatures depending on the damage parameters accumulation is also enclosed. The results are aimed to illustrate the influence of occuring damages of different type (damages in shear, tension and delamination) on the behavior of shear and tensile strains under different rates of loading. The sharp differences in strains on switching on the damage parameters make it possible to determine the values of damage parameters [2] ensuring coincidence of theoretical and experimental curves for shear and tensile strains under different rates of loading. The strain history is given for each rate of loading for the cases accounting for and neglecting the accumulation of damages, illustrating the differences in dynamical behavior of materials.

5.1 Twisting thin-walled tubular samples at different rates

In pure twisting of tubular samples by a rotating moment the shear stress $\sigma_{\theta z}$ was assumed to change linearly (Chapter 4):

$$\sigma_{\theta z}(t) = f \cdot t. \tag{5.1}$$

The experimentally measurable values $\varepsilon_{\theta z}$ and T under these conditions can depend only on damages in shear

$$(\alpha)$$

and delamination (ω_Δ). Now we will illustrate the solution of the direct problem: choosing the model composite material with given values of all the parameters we will determine variations of strains and temperatures under different rates of loading. That will help us to determine the necessary experiments for the solution of the inverse problem of developing the material parameters.

The values of parameters for the model composite material are given in the table 5.1. All the parameters were maintained constant. Only the twisting stress rate f (5.1) varied from 10^5 Pa/s to 10^9 Pa/s.

Parameter	Value	Unit	Description
c	0.61	–	matrix (phase 1) share in composite
T_0	300	K	initial temperature
ρ_1	1600	kg/m^3	density of the phase 1
ρ_2	1300	kg/m^3	density of the phase 2
μ_1	$53 \cdot 10^9$	Pa	shear modulus of the phase 1
μ_2	$1.98 \cdot 10^9$	Pa	shear modulus of the phase 2
λ_1	$94 \cdot 10^9$	Pa	adiabatic Lamè Lambda coefficient of the phase 1
λ_2	$7.54 \cdot 10^9$	Pa	adiabatic Lamè Lambda coefficient of the phase 2
$c_s^{(1)}$	1000	J/(kg·K)	specific heat capacity of the phase 1
$c_s^{(2)}$	2000	J/(kg·K)	specific heat capacity of the phase 2
$\alpha_v^{(1)}$	$2 \cdot 10^{-5}$	K^{-1}	volumetric thermal expansion modulus (phase 1)
$\alpha_v^{(2)}$	$1.5 \cdot 10^{-4}$	K^{-1}	volumetric thermal expansion modulus (phase 2)
τ_1	900	s	relaxation time of the phase 1
τ_2	10	s	relaxation time of the phase 2
Ω	25	s^{-1}	Omega (tensile damage) kinetic factor
C	25	s^{-1}	Alpha (shear damage) kinetic factor
D	25	s^{-1}	Omega-Delta (delamination damage) kinetic factor
Λ	$3 \cdot 10^8$	Pa·s	Omega enthropy factor
A	$3 \cdot 10^8$	Pa·s	Alpha enthropy factor
Λ_Δ	$3 \cdot 10^8$	Pa·s	Omega-Delta enthropy factor
ε_*	0.01	–	critical strain factor
ε_τ^*	0.01	–	critical shear factor
Δ_*	0.005	–	critical phases fitness factor
f	$10^5 \div 10^9$	Pa/s	twisting process stress per time factor
f	$10^5 \div 10^{10}$	Pa/s	straining process stress per time factor

Table 5.1. Parameters for the model composite

The results for the rate $f = 10^5$ Pa/s are illustrated in Fig. 5.1(a-d). The strain $\varepsilon_{\theta z}$ grows slowly (Fig. 5.1a) until damage parameter ω_Δ starts accumulating (Fig. 5.1c). Then $\varepsilon_{\theta z}$ starts growing much faster. The corresponding time t^*, strain $\varepsilon_{\theta z}^*$ and stress

$\sigma^*_{\theta z} = ft^*$ can be easily detected since from $t = t^*$ the behavior of $\varepsilon_{\theta z}(t)$ curve differs sharply from that in the absence of delamination ($\omega_\Delta \equiv 0$, see the dashed curve in Fig. 5.1a). The other damage parameter α remains zero under these loading conditions (Fig. 5.1b). The temperature variations ΔT are shown in Fig. 5.1d. While all the damage parameters are equal to zero ΔT turns to be slightly negative in deforming but those negative values cannot be distinguished within the scale of the figure. But on accumulation of the damage parameters (ω_Δ in the present case) the temperature grows rapidly in irreversible transformations (Fig. 5.1d).

The Figs. 5.2a-d illustrate the behavior of parameters under the rate of loading $f = 10^6$ Pa/s. It is seen that in faster loading the growth of ω_Δ starts earlier but brings to similar picture (Fig. 5.2a). The dashed curve on the Fig. 5.2a shows the behavior of $\varepsilon_{\theta z}$ in the absence of delamination. Damages in shear have not occured yet (Fig. 5.2b). Temperature variarions (Fig. 5.2d) are higher under these loading conditions.

Under even faster loading (Fig. 5.3; $f = 10^7$ Pa/s) the picture is qualitatively the same. Only the accumulation of damages in delamination starts much earlier and the critical values of $\varepsilon^*_{\theta z}$ and $\sigma^*_{\theta z}$ are higher for the present case than that for the previous cases. This result shows that under higher rates of loading the critical breakup limits turn to be higher.

Thus we can have a number of experiments under low rates of loading to determine the critical values $\varepsilon^*_{\theta z}$, $\sigma^*_{\theta z}$ for developing damage parameters and validation of results. The results for temperature variations can be also used for developing the model parameters and validating purposes.

The increase of the loading rate ($f = 10^8$ Pa/s) radically changes the scenarium of the process (Fig. 5.4). The rapid growth of strain $\varepsilon_{\theta z}$ starts much earlier due to accumulation of damages in shear (Fig. 5.4a); the dashed curve illustrates the strain $\varepsilon_{\theta z}$ behavior in the absence of shear damages accumulation. The damage parameter α grows very rapidly (Fig. 5.4b) while the damage parameter ω_Δ remains zero (Fig. 5.4c). The damages in delamination have not enough time to proceed since damages in shear bring to breakup very fastly. The temperature growth (Fig. 5.4d) takes place due to irreversible transformations in shear damaging.

The further increase of loading rate ($f = 10^9$ Pa/s) does not change the scenarium qualitatively (Fig. 5.5). The critical values $\varepsilon^{**}_{\theta z}$ and $\sigma^{**}_{\theta z} = f \cdot t$ for the present case can be determined as well and they turn to be higher than that for the previous case (Fig. 5.4a). Those critical values enable to develop the damage parameters responsible for damages in shear solving the inverse problem of developing model parameters based on the results of experiments.

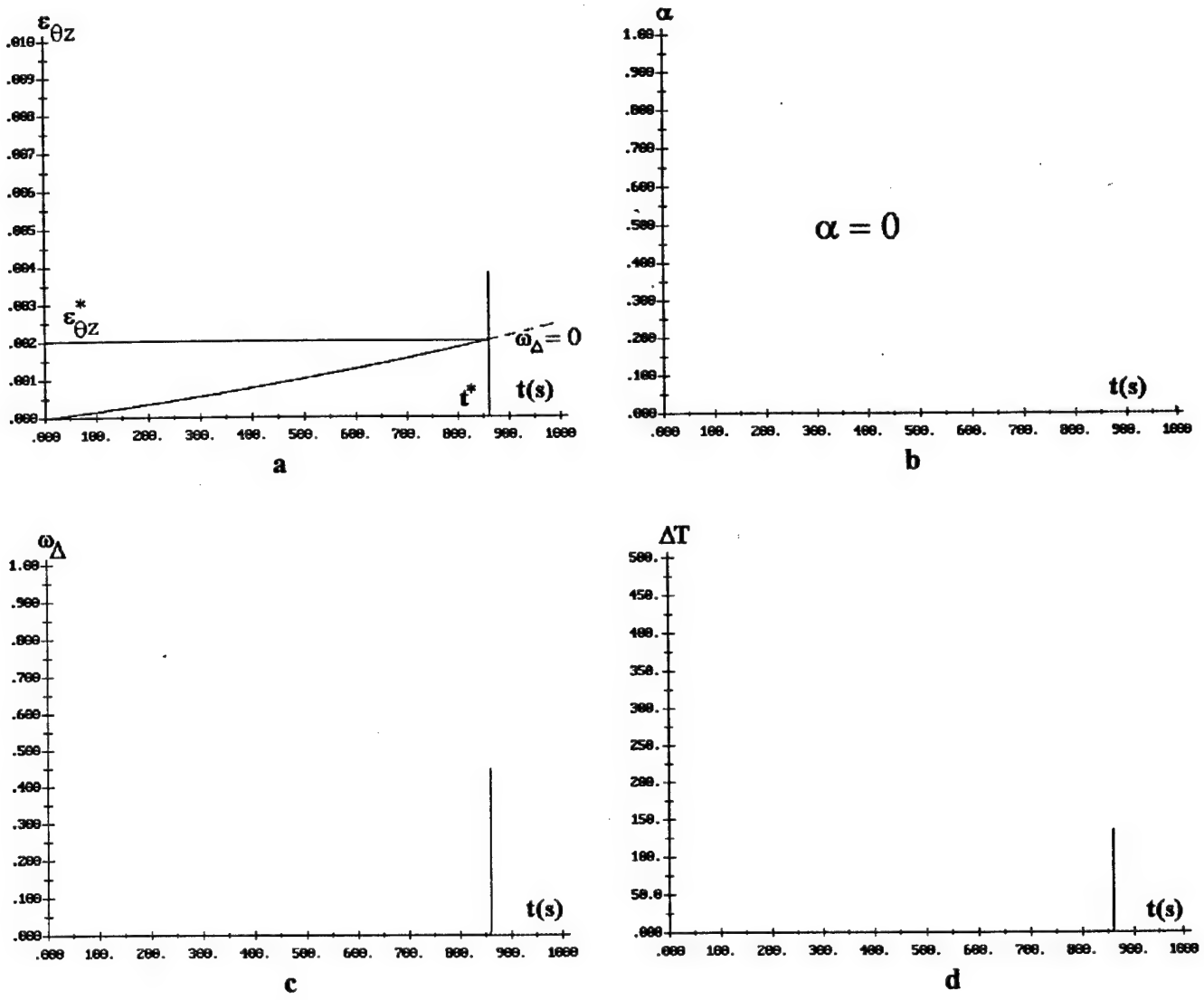

Fig. 5.1 Twisting of a tubular sample at $f = 10^5 \, Pa / s$.

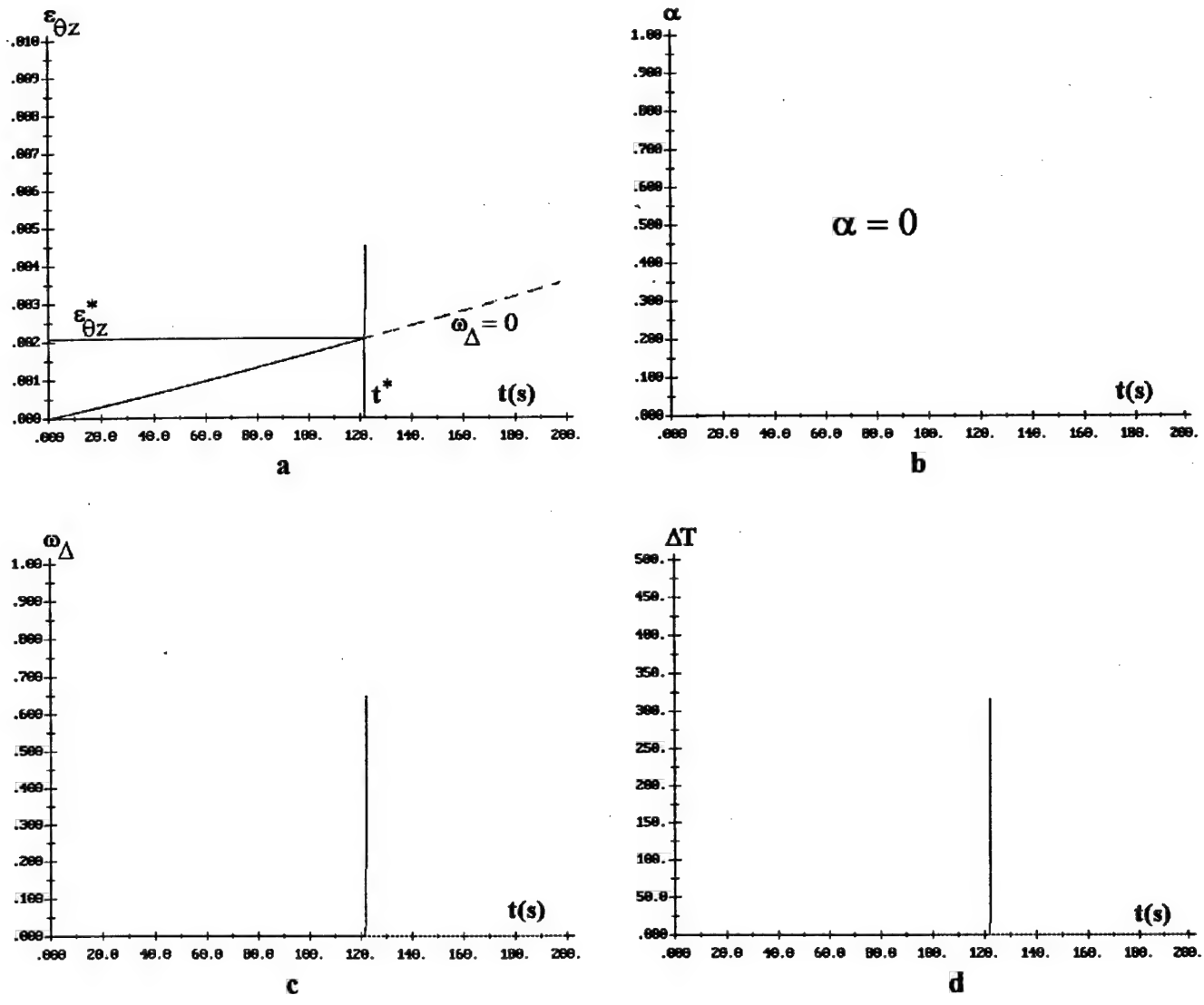

Fig. 5.2 Twisting of a tubular sample at $f = 10^6\,Pa/s$.

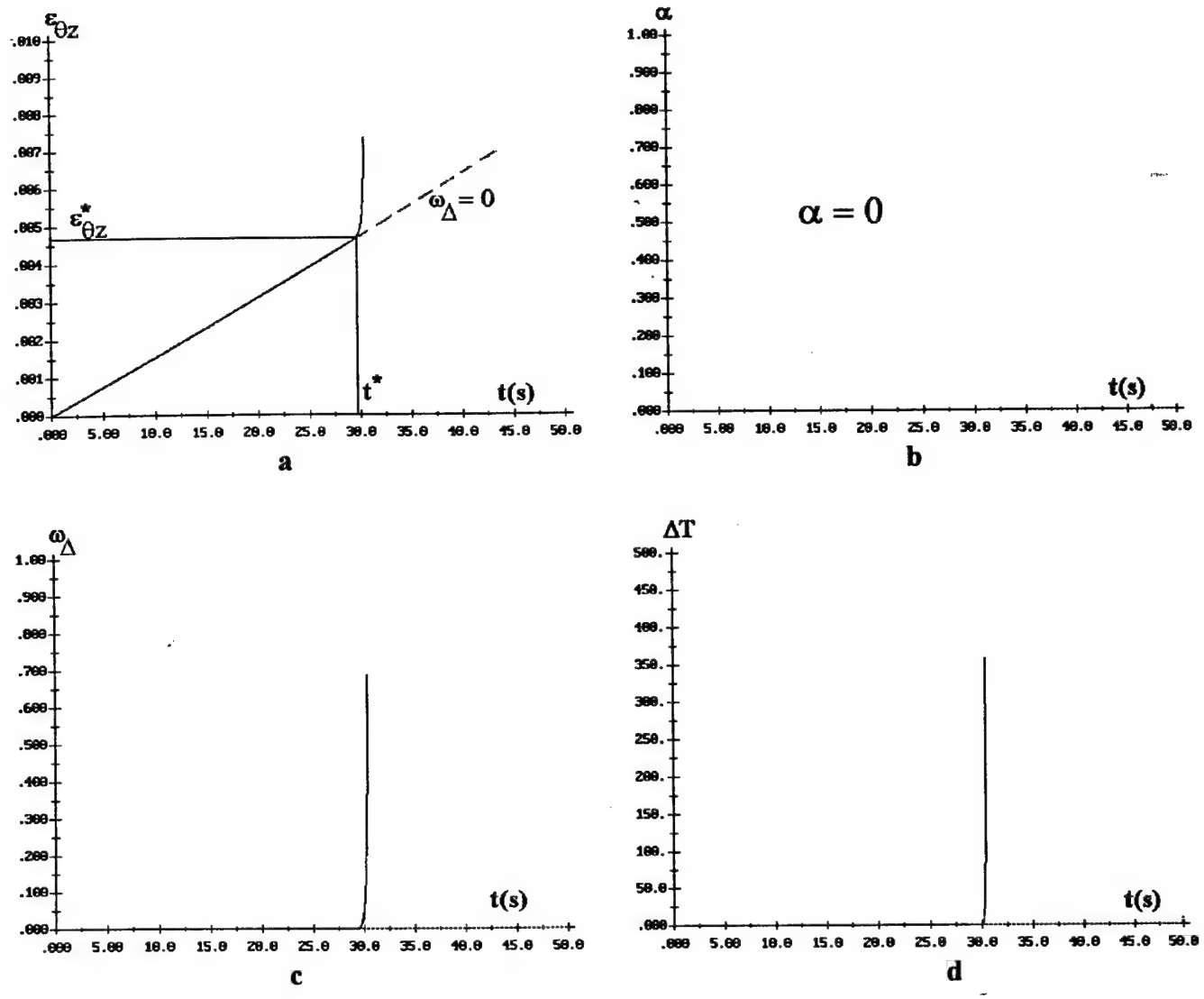

Fig. 5.3 Twisting of a tubular sample at $f = 10^7 \, Pa / s$.

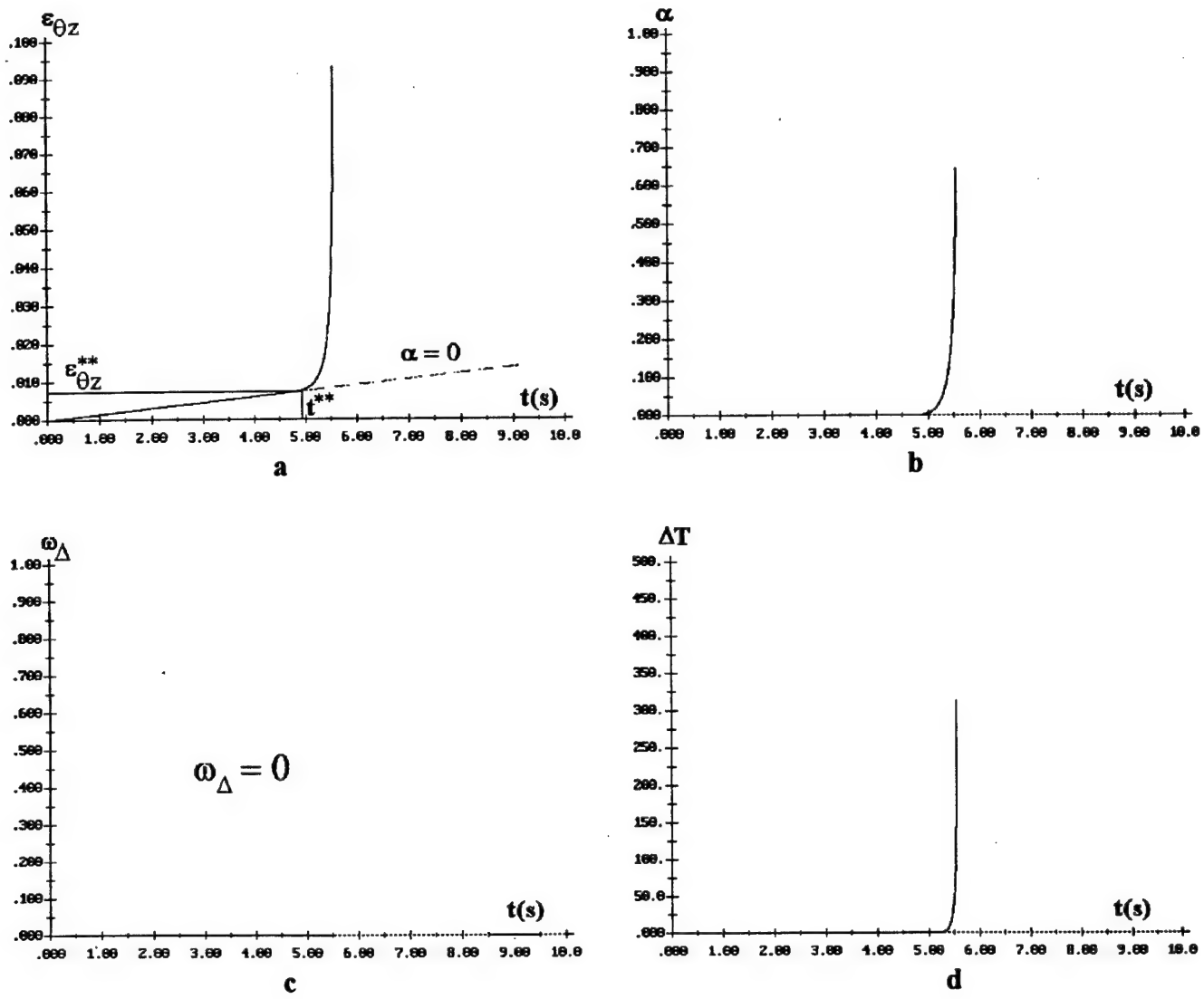

Fig. 5.4 Twisting of a tubular sample at $f = 10^8$ Pa / s .

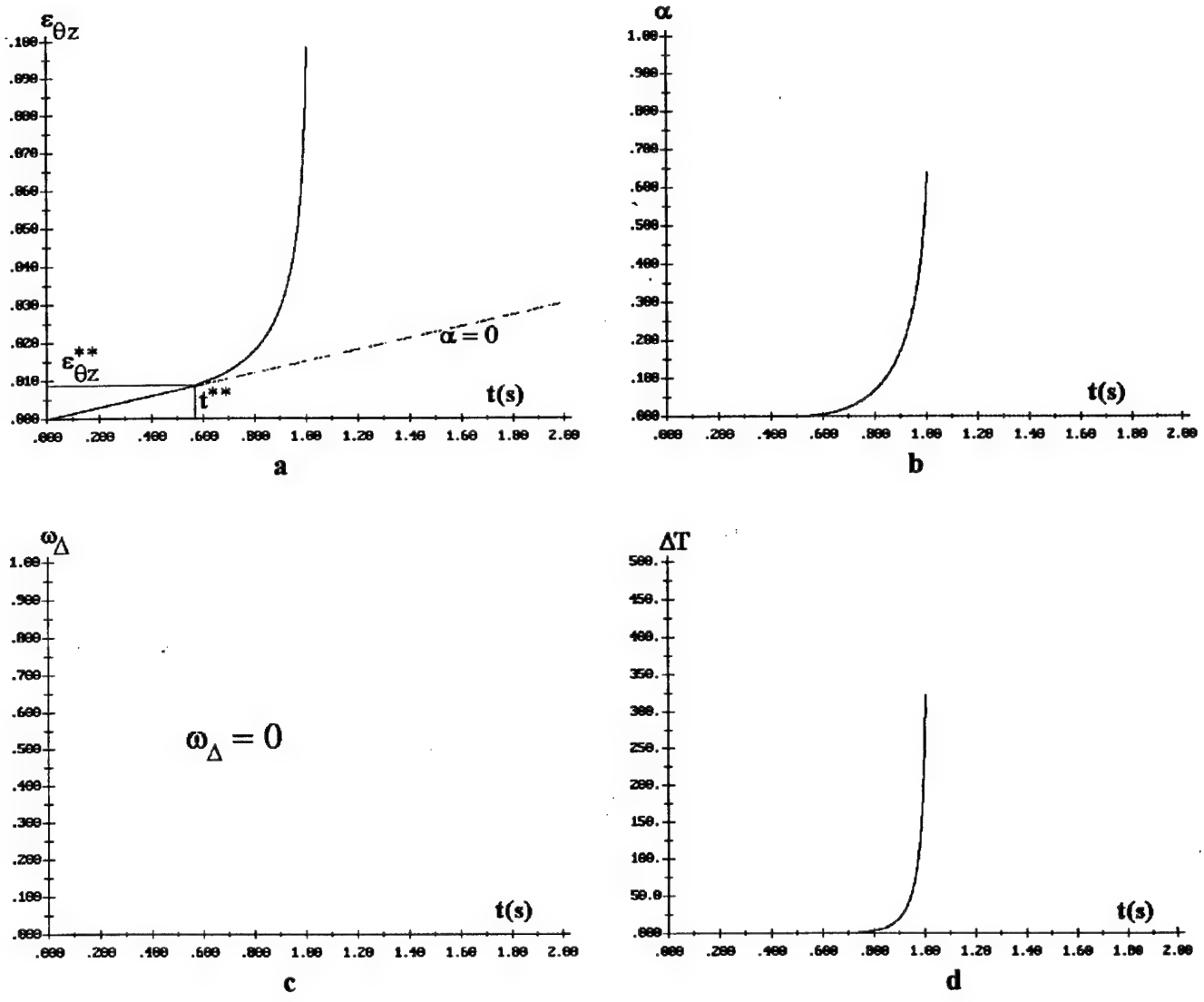

Fig. 5.5 Twisting of a tubular sample at $f = 10^9$ Pa / s.

5.2 Tension of a tubular sample

In pure tension of samples the only component of the stress tensor different from zero is assumed to change linearly:

$$\sigma_{zz}(t) = f \cdot t. \tag{5.2}$$

The experimentally measured values $\sigma_{zz}(t)$ and $T(t)$ depend on all the damage parameters under these conditions: damages in tension ω, in shear α and delamination ω_Δ.

The low rate of loading ($f = 10^5$ Pa/s) brings to the case of slow long-lasting growth of ε_{zz} (Fig. 5.6a) that is changed for a rapid growth when delamination occurs (Fig. 5.6c). The dashed curve on the Fig. 5.6a shows the behavior of ε_{zz} in the absence of delamination. The other damage parameters remain constant (Figs. 5.6b,d). Temperature variation in irreversible transformations is relatively not very high (Fig. 5.6e). The critical values of ε^*_{zz}, $\sigma^*_{zz}(t^*) = f \cdot t^*$ can be determined from the picture. In solving the inverse problems of developing the damage constants from experiments the values σ^*_{zz}, ε^*_{zz} can be used for validating the damage in delamination constants determined in the experiments on twisting the sample.

The increase of the rate of loading ($f = 10^6$ Pa/s) does not change the picture qualitatively, but quantitatively decreases the breakup time and increases the critical values ε^*_{zz} and σ^*_{zz} (Fig. 5.7). The damage parameters α and ω remain equal to zero (Figs. 5.7b,d) since the critical values ε^*_{zz} and σ^*_{zz} are still much lower than that necessary for damages in tension and shear to proceed.

The increase of loading rate up to $f = 10^7$ Pa/s does not change the scenarium qualitatively (Fig. 5.8) but brings to essential quantitative changes. The critical values ε^*_{zz} and σ^*_{zz} grow up and approach ones under which the damages in shear and tension can occur.

The future increase of the loading rate ($f = 10^8$ Pa/s) brings to the scenarium when breakup is achieved due to growth of damages in shear (Fig. 5.9b) and tension (Fig. 5.9d). The rapid growth of ε_{zz} followed by the breakup (Fig. 5.9a) takes place very quickly so that damage in delamination cannot occur (its critical parameters ε^*_{zz} and σ^*_{zz} under the present loading conditions are higher than that for damages in shear (ε^{**}_{zz} and σ^{**}_{zz}) and tension (ε^{***}_{zz} and σ^{***}_{zz}).

The dashed curve on the Fig. 5.9a marked "$\alpha = 0$" shows the behavior of ε_{zz} in the absence of shear damages accumulation; it is placed very near to the actual ε_{zz} curve (solid line), that means that the breakup under present loading conditions occurs mostly because of tensile damages accumulation, and the accumulation of damages in shear practically does not influence the breakup scenarium. The dashed curve on the Fig. 5.9a marked "$\omega = 0$" shows the behavior of ε_{zz} in the absence of tensile damages; it separates from the dashed curve marked "$\alpha = \omega = 0$" later. Comparison of the dashed curves marked "$\omega = 0$" on the Figs. 5.9b,c,d shows that in case of neglecting the tensile damages accumulation the breakup will be delayed, and both shear and delamination will take place. However the delamination does not take place when we account for the the tensile damages.

Damages in tension occur a little bit earlier than in shear (Fig. 5.9d) and their growth

brings to strong changes in $\varepsilon_{zz}(t)$ function behavior. At the same time, the successive growth of the α-parameter does not bring essential changes to the growth of the ω-parameter (Fig. 5.9d), ε_{zz} strain and temperature under the present loading conditions. The dashed curve marked "$\alpha = 0$" in Fig. 5.9d shows the growth of ω under the condition of α (shear damages accumulation) remaining zero.

The critical strains ε_{zz}^{***} and stress σ_{zz}^{***} can be determined from Fig. 5.9a.

In solving the inverse problem the critical values determined from the experimental curve $\varepsilon_{zz}(t)$ could be used for developing the model constants for damages in tension (Ω, Λ, ε_*) since the model parameters for damages in shear could be determined from the experiments on twisting the samples (section 5.1).

Fig. 5.10 illustrates the results for the higher rate of loading $f = 10^9$ Pa/s. It is seen that accumulations of both damage parameters α and ω contribute to the rapid growth of ε_{zz} after the critical values are reached (Fig. 5.10a). The absence of one of the damage parameters α or ω essentially influences the growth of the other (Figs. 5.10b,d). The growth of temperature under present rate of loading takes place mostly due to the growth of α (damages in shear).

The further increase of the rate of loading ($f = 10^{10}$ Pa/s) does not change the picture qualitatively but brings to an increase of the critical values of ε_{zz}^{***} and $\sigma_{zz}^{***} = f \cdot t^{***}$ and to a decrease of characteristic breakup time. The results for the rate of loading $f = 10^{10}$ Pa/s are shown on the Fig. 5.11a-e.

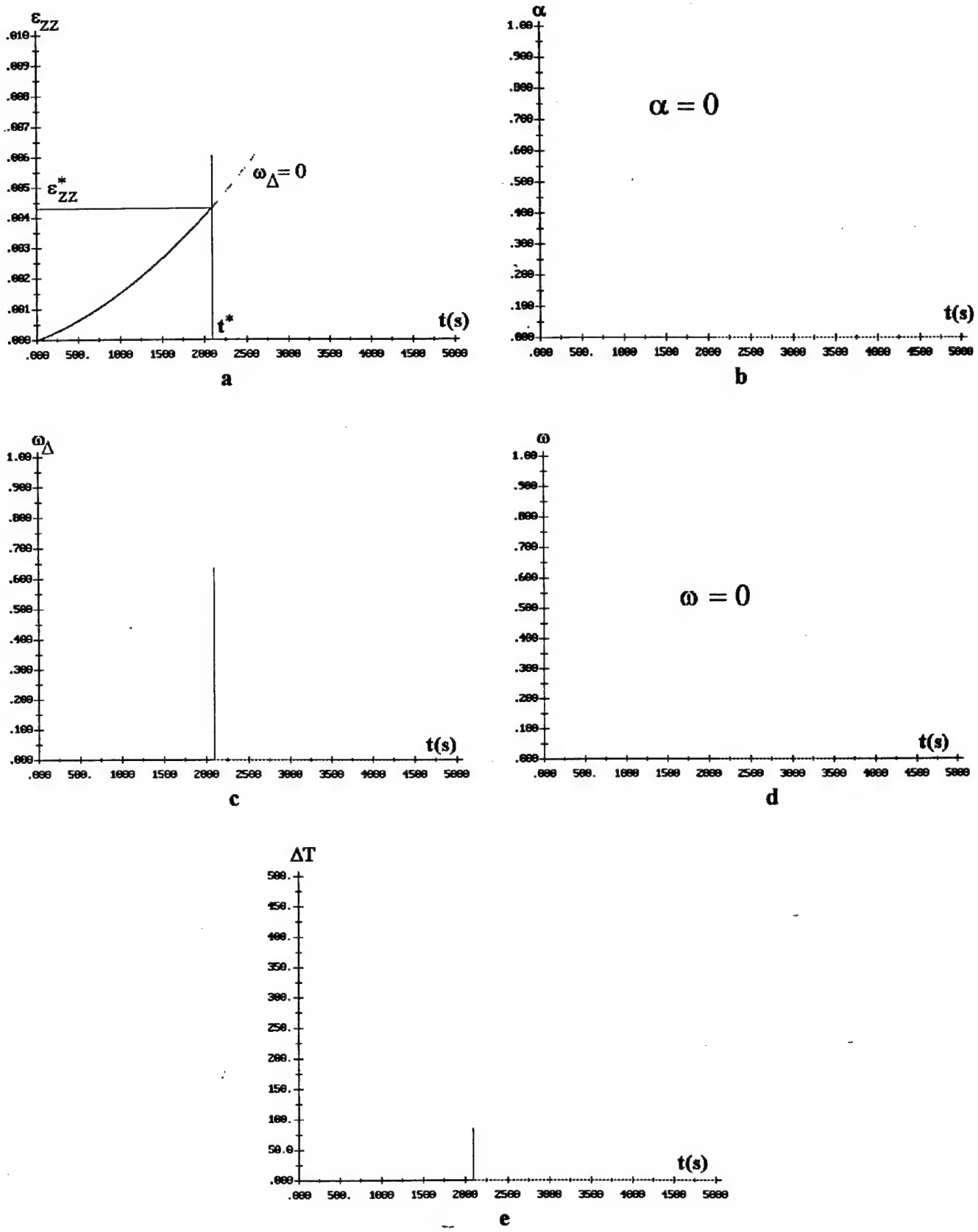

Fig. 5.6 Tension of a tubular sample at $f = 10^5 \, Pa / s$.

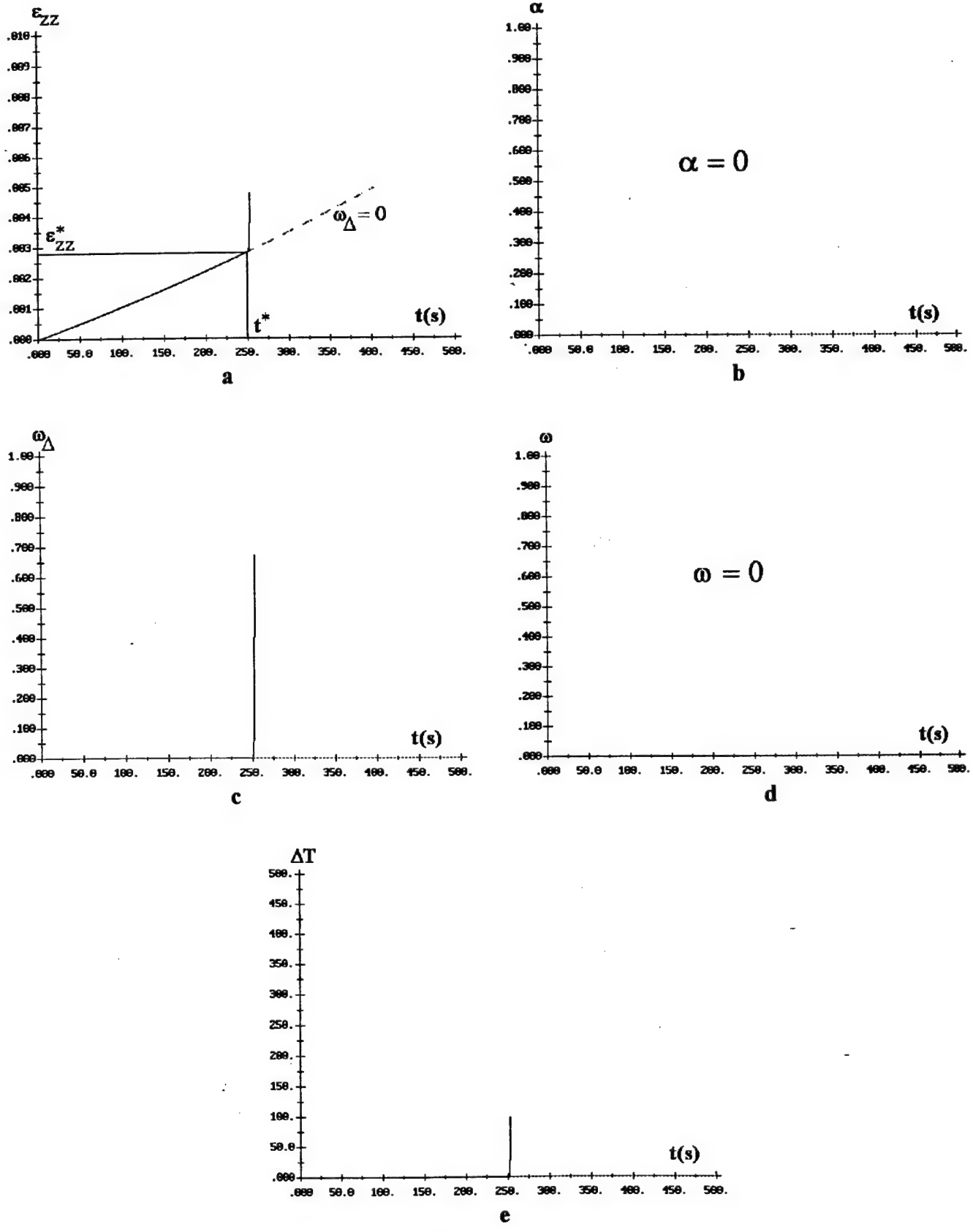

Fig. 5.7 Tension of a tubular sample at $f = 10^6 \, Pa / s$.

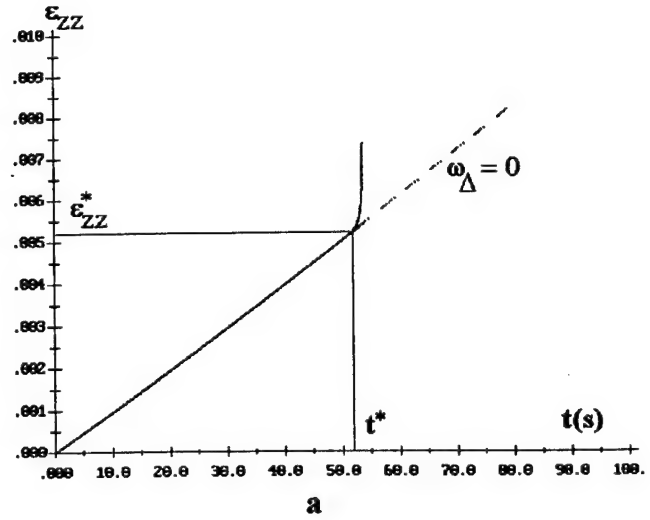

a

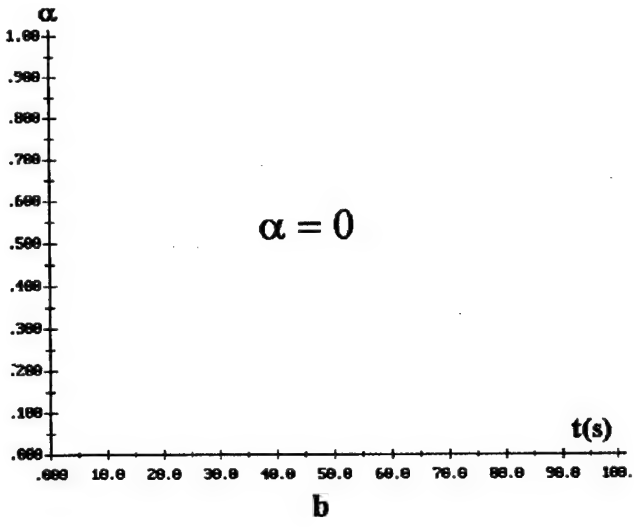

b

Straining the tubular sample

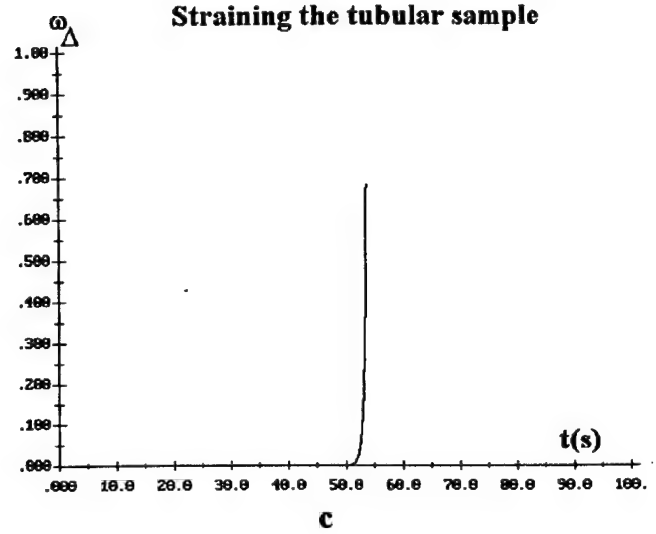

c

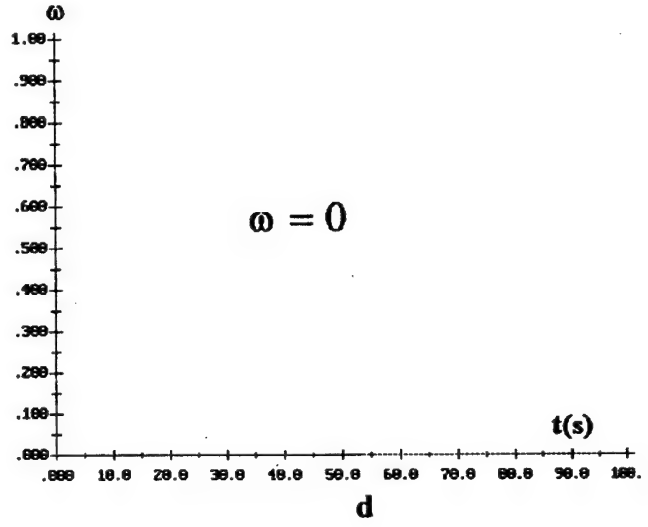

d

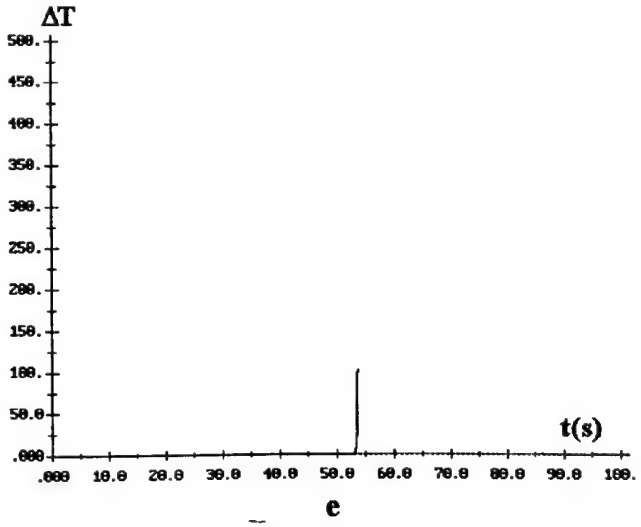

e

Fig. 5.8 Tension of a tubular sample at $f = 10^7 \, Pa/s$.

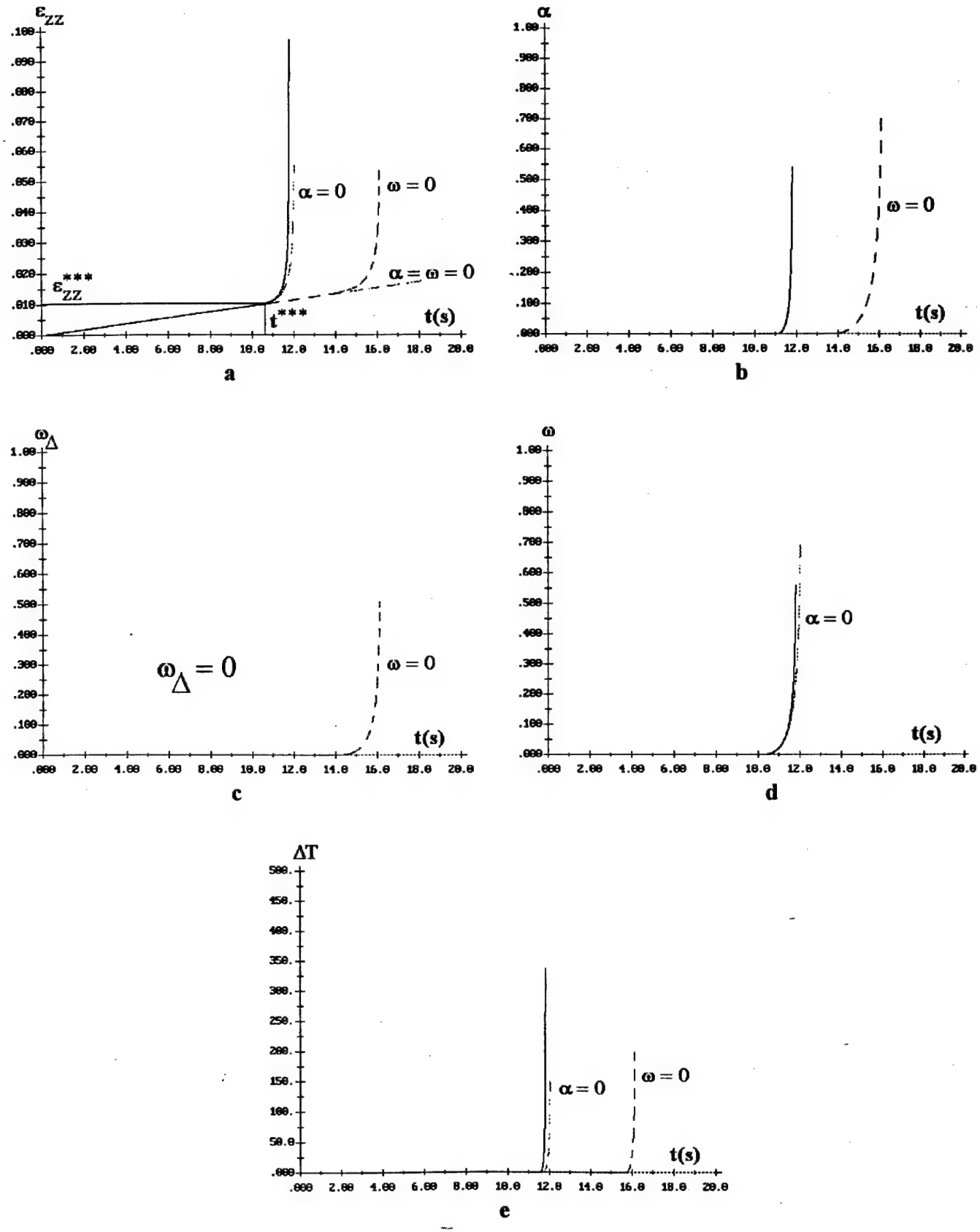

Fig. 5.9 Tension of a tubular sample at $f = 10^8$ Pa / s.

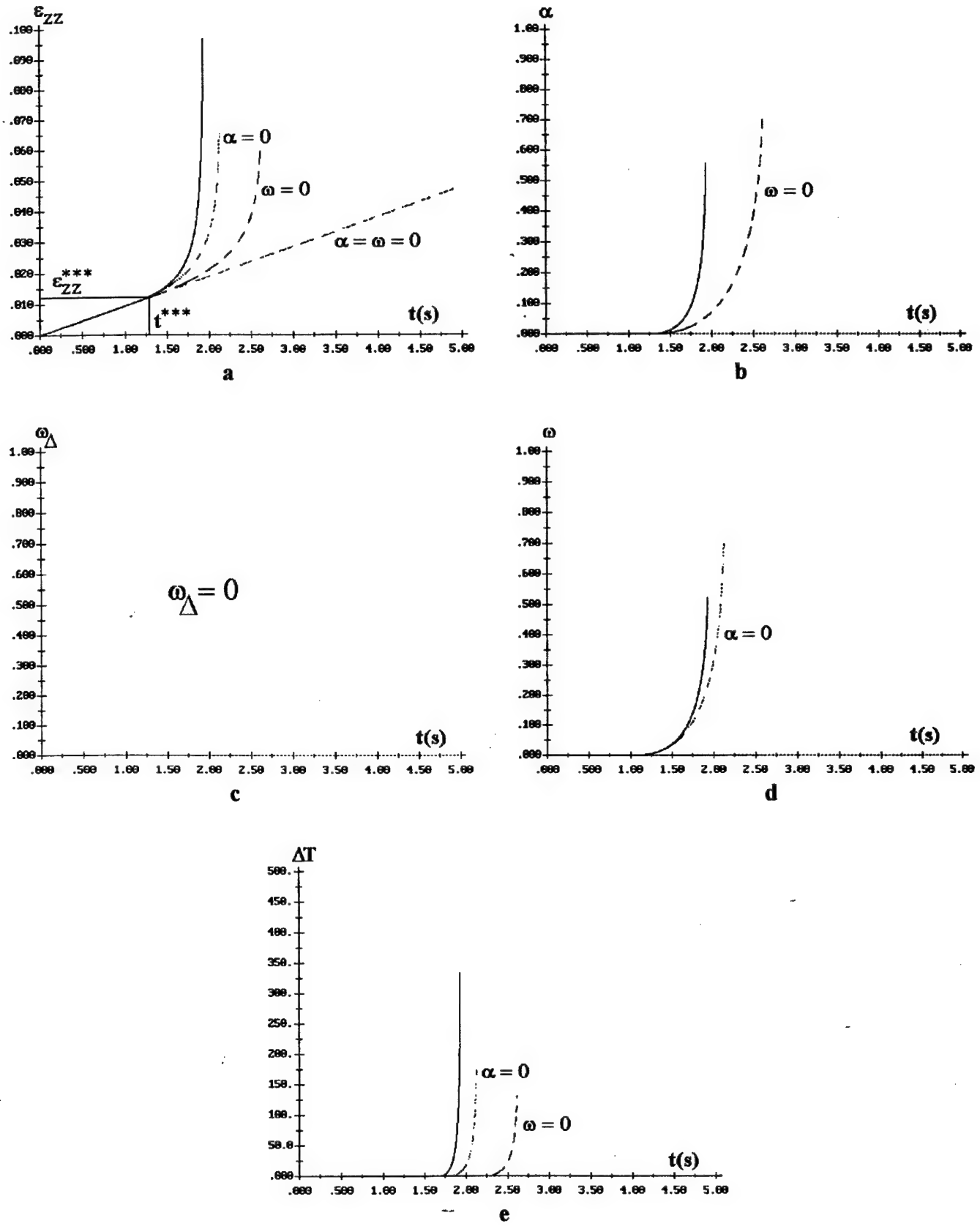

Fig. 5.10 Tension of a tubular sample at $f = 10^9$ Pa / s.

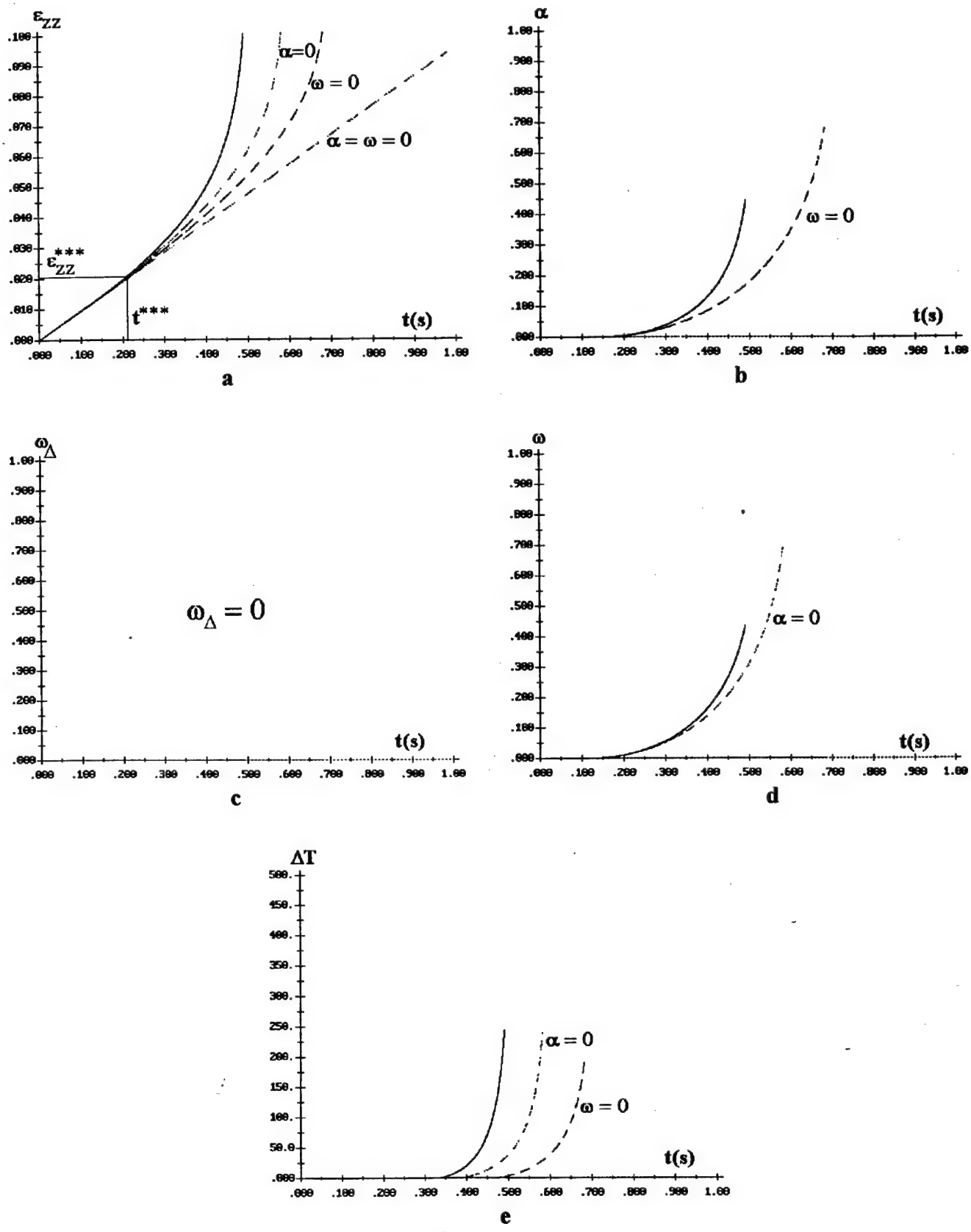

Fig. 5.11 Tension of a tubular sample at $f = 10^{10}\,Pa/s$.

5.3 Recommendations on developing the model damage constants in experiments

The numerical simulations of dynamical behavior of parameters in twisting and tension of tubular composite samples shown definite peculiarities of scenario for the materials posessing the properties close to that given in the table 5.1.

For the low rates of loading both in twisting and tension the breakup takes place due to accumulation of damages in delamination while the damage parameters in shear and tension remain equal to zero. Thus the critical values for parameters $\varepsilon^*_{\theta z}, \varepsilon^*_{zz}, \sigma^*_{\theta z}, \sigma^*_{zz}$ can be determined from the experimental strain–time diagram enabling to develop the damage constants D, Λ_Δ, Δ_*. The experimental results under different rates of loading can be used for validating purposes.

For the high rates of loading in twisting the breakup takes place due to accumuation of damages in shear, and for the loading in tension – due to accumulation of damages both in shear and tension, while the damage parameter ω_Δ remains equal to zero. Thus the critical values $\varepsilon^{**}_{\theta z}, \sigma^{**}_{\theta z}$ can be determined from the experiments in twisting. Different rates of loading can provide with different pairs of $\varepsilon^{**}_{\theta z}, \sigma^{**}_{\theta z}$ that would make it possible to determine the damage constants for the damage in shear: C, A, ε^*_τ. The experimental data on temperature growth ΔT can provide with additional data for developing those constants and validation.

Experiments in high rate tension can provide with the critical parameters $\varepsilon^{***}_{zz}, \sigma^{***}_{zz}$ characterizing the beginning of damaging in tension. Assuming the model constants for the shear damages known from independent experiments in twisting one can develop the model constants $\Omega, \Lambda, \varepsilon_*$ for the damages in tension based on the experimental $\varepsilon_{zz}(t)$ and $T(t)$ curves.

Chapter 6

On the methods of modeling the material behavior after destruction criteria having been satisfied in some zones

Intensive dynamic loading of the structure elements (in impact, explosion or thermal loading) brings to destruction of materials. Dynamical breakup is a complex multistage process involving origination, growth and coalescence of microdefects, formation of microcracks, their growth to macroscale, intersections leading to fragmentation of material.

Two characteristic stages can be distinguished within the process of dynamical breakup. The first stage – predestruction (continual, or uniformly distributed destruction) : origination of microdefects, their growth and coalescence, formation of initial macrocracks and pores in the process of irreversible deformation of material.

The second stage – destruction of material : formation of macrocracks and growth of pores inside the material, their coming to free surface, separation of fragments.

Mathematical modeling of the predestruction stage can be performed introducing damage parameters for materials. Models of this type applied for two-phase laminated composite materials were described in [1,2] and are discussed in the chapters 4 and 5 of the present report. After the destruction criteria for the critical specific dissipation is satisfied in some place

$$D = D_*, \tag{6.1}$$

the present computation cell gives birth to a new destruction interface free of loadings (in case the destruction criterion (6.1) was not satisfied in the adjacent cells before). Otherwise the crack born in the adjacent cell should grow through the present cell.

Here we regard the approaches to mathematical modeling of the second stage of destruction. There exist at least two different approaches [3-6]. The first one is based on the explicit tracking of the free surfaces of the crack. The second is replacing the destructed material by a number of discrete particles characterized by their sizes, mass and

momentum. Those particles can interact with each other and with the free surfaces of the continuous material following a given law.

The second approach is not in fact an alternative to the first one but rather its further development. The second approach permits to create a simplified procedure for numerics: the destructed material is assumed to be a media resisting compression but irresistible for expansion in tension. In a number of cases this simplification is significant for practical applications.

Further we regard the both approaches taking a two-dimensional case as an example.

6.1 The method of explicit free surface tracking in macroscopical destruction of material

Using the Lagrangian approach for description of the media deformation the cells move with the media. Thus the most effective method of free surface tracking is based on the local reconstruction of the grid in the zone of the crack [3-6]. On giving birth to a crack the cell is removed from the grid and replaced by the two free surfaces on the both sides of the gap. The mass, momentum and other characteristics of the cell are redistributed among the adjacent ones. The both sides of the crack are either free of tensions or have the "contact" boundary conditions depending on the process. If the crack is expanding a free surface boundary conditions are applied. In case of the collapse of the gap the calculations are conducted using the contact boundary conditions algorithm [7].

The basic ideas of the method will be discussed using an example of modeling the border surfaces of an arbitrary curved crack in a continuum.

Let the conditions for macrodestruction (6.1) be satisfied in some cell of the grid. The first alternative to be checked under conditions is either birth of a new crack takes place or the further propagation of a crack existing in the adjacent cell. In other words, we check if all the adjacent cells are not destructed.

I. In case of a new crack is being born in the cell the following algorithm is applied:

1) The center if the cell where the destruction criterion (6.1) was satisfied is determined:

$$x_1^c = \frac{1}{4}\sum_{k=1}^{4} x_1^k; \qquad x_2^c = \frac{1}{4}\sum_{k=1}^{4} x_2^k,$$

$k = 1, 2, 3, 4$ – numbers of the grid points surrounding the cell (Fig. 6.1). The procedure is performed in the laboratory system of coordinates $\{x_1, x_2\}$.

2) The orientation of the gap plane in the center of the cell is determined. The orientations of the planes of maximal orthogonal σ_n and tangential σ_τ stresses are determined for the purpose as well as their values within the cell:

$$\sigma_n = \sigma_{11}\alpha^2 + 2\sigma_{12}\alpha\beta + \sigma_{22}\beta^2;$$

$$\sigma_\tau = \sqrt{|\vec{\sigma}_n|^2 - \sigma_n^2} = \sqrt{(\sigma_{11}\alpha + \sigma_{12}\beta)^2 + (\sigma_{12}\alpha + \sigma_{22}\beta)^2 - \sigma_n^2};$$

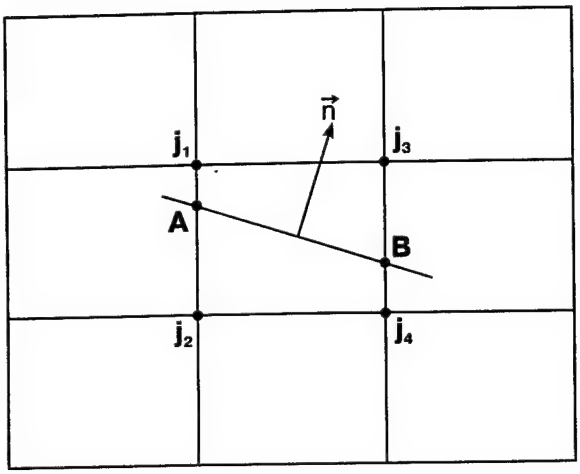

Fig. 6.1.

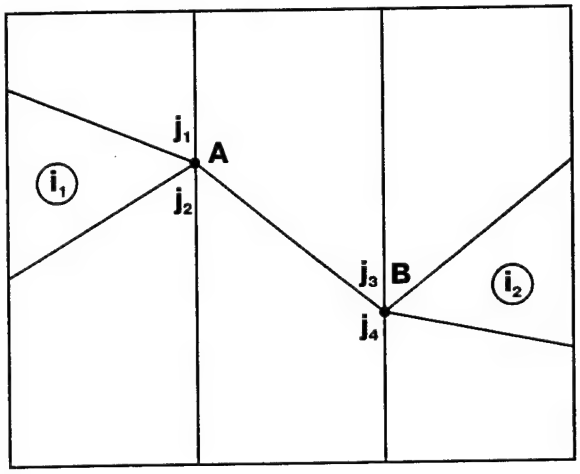

Fig. 6.2.

$$\alpha^2 + \beta^2 = 1;$$

where $\vec{n} = (\alpha, \beta)$ – a unit normal vector to the plane of maximal stresses (Fig. 6.1). The procedure described above enables to determine two planes characterized by normal vectors $\vec{n}_n = (\alpha_n, \beta_n)$ and $\vec{n}_\tau = (\alpha_\tau, \beta_\tau)$. The first one $(\vec{n}_n)$ is that of maximal normal stress σ_n in the cell, the second one $(\vec{n}_\tau)$ is the plane of maximal tangential stresses σ_τ. So one has an alternative of two probable orientations of the originating crack. The following criterion permits to make the choice of the direction of the crack:

$$\max\left(\frac{\sigma_\tau}{\tau_B}, \frac{\sigma_n}{\sigma_B}\right),$$

where τ_B is the maximal shear limit, σ_B – maximal tensile limit (material constants).

If the condition

$$\frac{\sigma_\tau}{\tau_B} > \frac{\sigma_n}{\sigma_B}$$

is satisfied it is assumed that the shear crack is born within the cell along the plane characterized by the normal vector $\vec{n}_\tau$.

If the condition

$$\frac{\sigma_\tau}{\tau_B} < \frac{\sigma_n}{\sigma_B}$$

is satisfied within the cell the tensile crack is to be born along the plane characterized by the normal vector $\vec{n}_n$. The criterion formulated above is the classical one of Davidenkov-Friedmann.

3) The intersections of the crack plane with the grid lines surrounding the cell are determined (Fig. 6.1). Let the intersection A be on (j_1, j_2) and the intersection B be on (j_3, j_4).

4) The grid points j_1 and j_2 are moved into the point A, the grid points j_3, j_4 are moved into the point B (Fig. 6.2). All the parameters related to the grid points and the adjacent cells are relocated following the procedures described in [8]. The idea of the grid modification of this type is illustrated in the Fig. 6.2.

II. In case of propagation of the crack from an adjacent cell a different procedure is used. The Fig. 6.2 shows that the crack can propagate further either in the cell i_1 or in the cell i_2. There can take place more complicated cases that will be regarded later.

A. Let the crack grow into the cell i_1, i.e. the destruction criterion for the critical value of dissipation (6.1) is satisfied in the cell i_1. And the values of the normal vector to the plane $\vec{n} = (\alpha, \beta)$ are determined. Then the border interfaces of the crack in the i_1 cell can be determined in the following way.

1) Knowing the orientation of the crack plane in the cell i_1 one can construct the plane beginning from point C of its intersection with the border of the cell j_5, j_6 as shown in the Fig. 6.3.

2) The grid points j_5 and j_6 are moved to the point C. All the values of parameters, mass, momentum, energy in the cells i_3 and i_4 are redetermined following the new grid

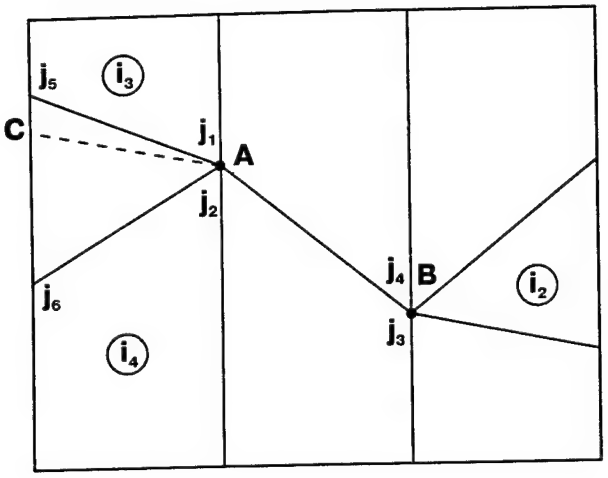

Fig. 6.3.

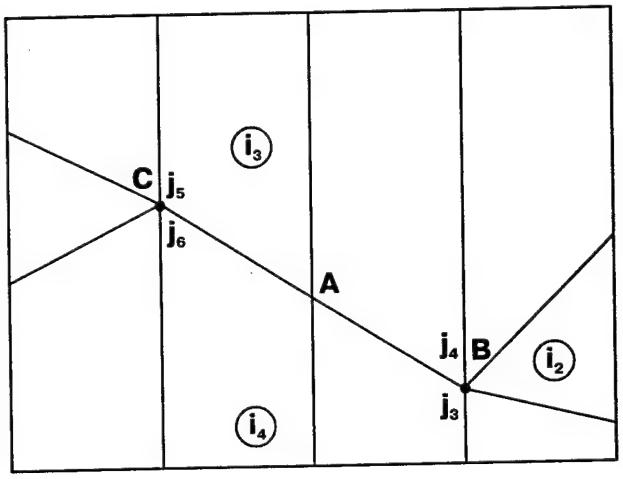

Fig. 6.4.

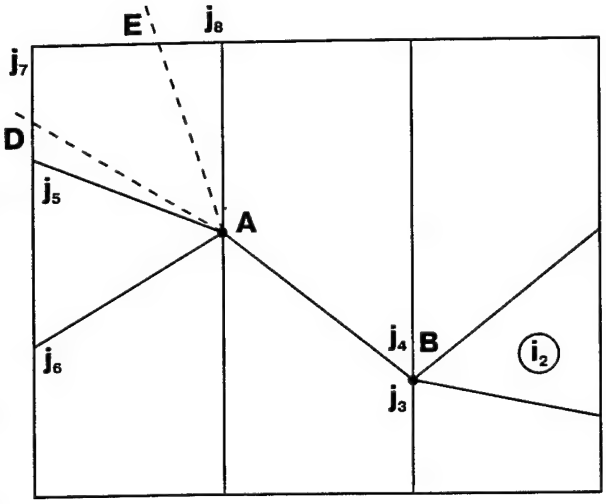

Fig. 6.5.

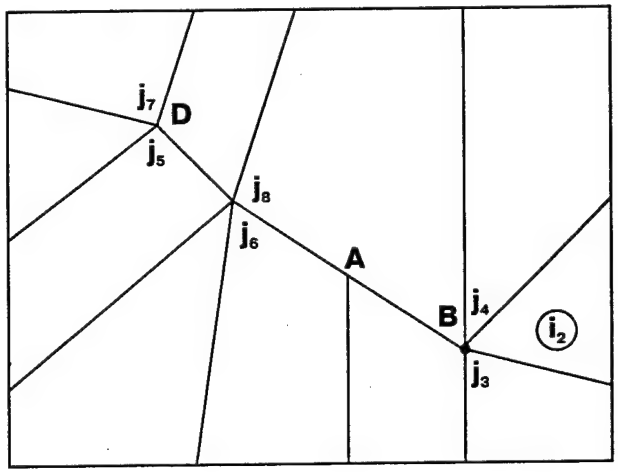

Fig. 6.6.

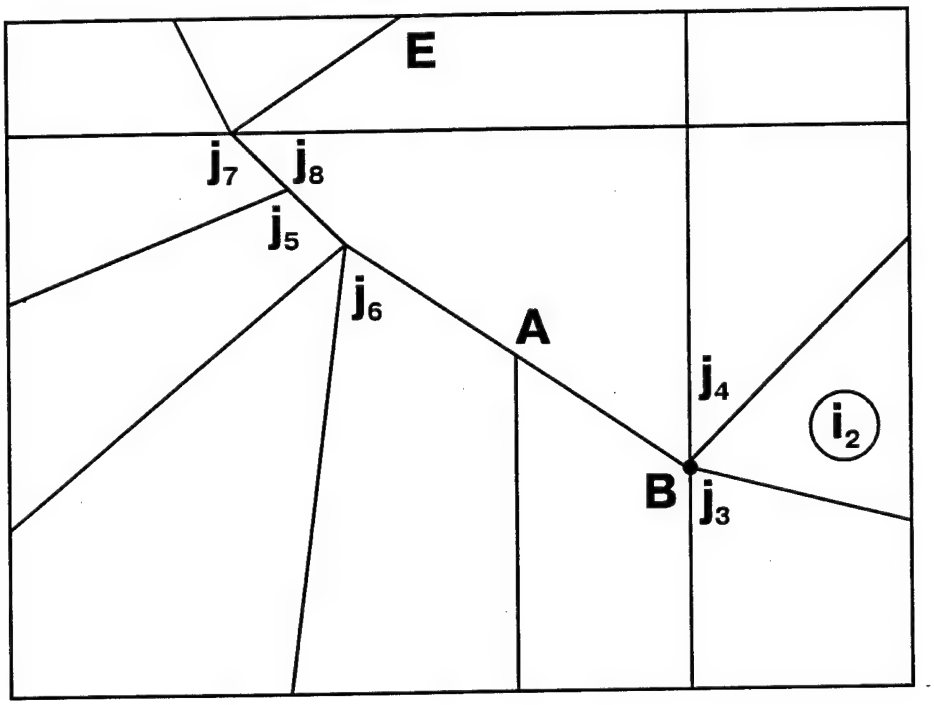

Fig. 6.7.

pattern. The Fig. 6.4 presents a fragment of the computational grid with a gap in two cells.

B. Let the crack due to determined orientation of maximal stresses planes grow outside the cell i_1 (Fig. 6.2) and cross the cell i_3 for example (Fig. 6.3). Then tracking the borders of the crack is performed by the following algorithm.

1) The gap plane is constructed beginning in the point A and tracked until it intersects with the borders of the cell i_3. Two cases are possible:

a) the point of intersection D is found on the border $j_5 j_7$ or

b) the point of intersection E is found on the border $j_7 j_8$ (Fig. 6.5).

2a) In case "a" the grid points j_5, j_7 are moved into the point D, the grid points j_6 and j_8 are moved into the center of AD. The new grid fragment after the reconstruction is shown in Fig. 6.6.

2b) In the opposite case "b" the grid points j_7 and j_8 are moved into the point E, the grid point j_5 is moved into the center of $j_5 A$ as shown in Fig. 6.7.

Thus successive satisfying the destruction criterion in the cells enables to track uniquely the macroscopical crack. In case the macroscopical crack comes to a free surface, separation of some part of material as a fragment is possible.

The precision of the described above procedure of localization of a crack is one half a mesh width.

6.2 Replacing the destructed material with descrete particles

Most of numerical algorithms are constructed in a way providing at each timestep the following data:

1) in every cell: density of material, stress, strain and strain rates tensors, specific internal energy, dissipation, temperature, damadge parameters (in case the model for damadgeable media is used);

2) in the grid points: velocities and current coordinates. Thus the first group of parameters is related to the centers of the cells, the second – to the grid points.

In case the destruction criterion (6.1) is satisfied in a cell the material in the cell is considered to be macroscopically damadged. To model the behavior of the material within the damadged cell it is assumed that the material resists the compression only and has no resistance to expansion and shear. That means the stress tensor for the damadged medium σ_{ij} is a spherical one: $\sigma_{ij} = -p\delta_{ij}$. The equation of state for pressure p within the damadged cell has the following form, for example:

$$p = \begin{cases} K\left(\dfrac{\rho}{\rho_*} - 1\right)^n, & \rho > \rho_* \\ 0, & \rho < \rho_* \end{cases} \tag{6.2}$$

where ρ_* is the density of the material within the cell by the time of destruction (the time for the criterion (6.1) is satisfied), K, n – material constants.

In case the damadged cell is an internal one, the calculations are run following the same algorithm but for the equation of state that needs to be taken in the form (6.2).

In case the damadged cell is at the boundary of the computational domain the material of the cell is replaced by a number of discrete particles with the radii determined from the condition fitting the cell. The mass of the cell is redistributed among the particles. Only one layer of the boundary cells can be transformed into discrete particles during one time step because it is assumed that the velocity of the destruction wave does not exceed the velocity of acoustic disturbances in the media.

Thus applying such an algorithm can lead in some cases to replacing all the cells with discrete particles, i.e. converting a continuous body into a cloud of fragments.

Velocity vectors for the mass points (grid points and discrete particles) are determined from the following finite-differences equations:

$$\frac{\vec{v}_i^{n+1} - \vec{v}_i^n}{\tau} = \frac{\vec{F}_i^n + \vec{R}_i^n}{2\varphi_i},$$

where i is the number of a grid point or a particle, n – the number of a time step, $2\varphi_i$ – mass of the respective mass point, τ – time step value, $\vec{F}_i^n$ – vector of forces caused by internal stresses, $\vec{R}_i^n$ – vector of reaction forces, that is equal to zero in the internal grid points and is determined or assigned for the boundary grid points.

Let us regard the most general case when the computational domain contains both the grid points and discrete particles. The discrete particles are assumed to be incompressible and interacting with the boundaries of the continuos medium and with each other. An elementary act of interaction of a fragment with the boundary of continuous media is modeled in the following way.

The known by the time $t = t^n$ values of coordinate vectors $\vec{x}_i^n$ and velocities $\vec{v}_i^n$ $(i = a, b, c)$ for the grid points "a", "b" and the discrete fragment "c" make it possible to determine intermediate values of coordinates and velocities $\vec{x}_i^{n+1}$, $\vec{v}_i^{n+1}$ (Fig. 6.8) not taking into account reaction forces. If the following condition is satisfied for the intermediate values

$$h = \frac{2S_{abc}}{l_{ab}} < r_c,$$

then the penetration of the particle "c" into the continuous material must have taken place. Then the corection of coordinate vectors and velocities for the grid points "a", "b" and the particle "c" is necessary. Here r_c is the particle's radius, l_{ab} – the distance between "a" and "b" grid points, h – the height of the triangle "abc". Under the condition $h > r_c$ there is no interaction of particle "c" with the boundaries of the continuous material.

To perform the corrections the random vector components being the result of interactions are determined. The friction forces are determined as well if the law is given. The grid points "a", "b" and the particle "c" are affected by the following forces:

$$\vec{R}_c = N_c\vec{n} + T_c\vec{\tau}, \quad \vec{R}_a = -(1-\alpha)\vec{R}_c, \quad \vec{R}_b = -\alpha\vec{R}_c, \tag{6.3}$$

where

$$N_c = \frac{[(1-\alpha)v_{na}^* + \alpha v_{nb}^* - v_{nc}^*]}{\tau\varphi^*}, \quad T_c = \frac{(1-\alpha)v_{\tau a}^* + \alpha v_{\tau b}^* - v_{\tau c}^*}{\tau\varphi^*},$$

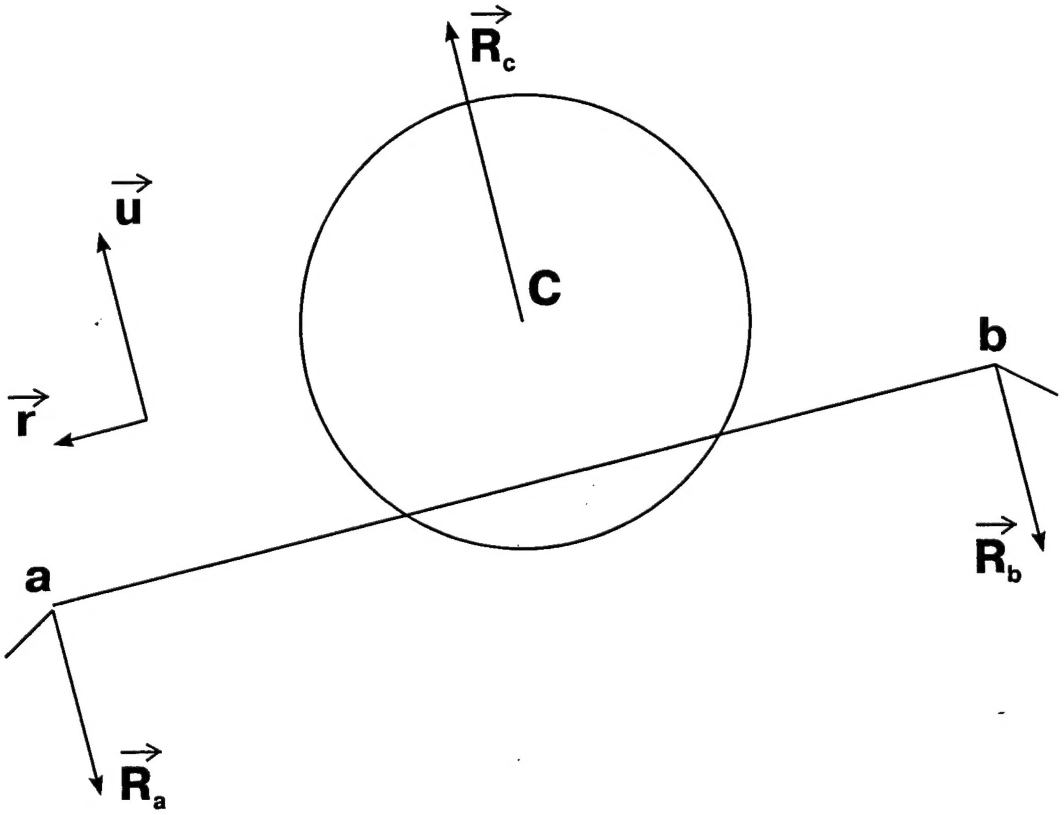

Fig. 6.8.

$$\varphi^* = \frac{1}{\varphi_c} + \frac{(1-\alpha)^2}{\varphi_a} + \frac{\alpha^2}{\varphi_b}, \quad \vec{\tau} = \frac{\vec{x}_a^* - \vec{x}_b^*}{l_{ab}^*},$$
$$l_{ab}^* = |\vec{x}_a - \vec{x}_b|, \quad \alpha = l_{ak}^*/l_{ab}^*, \quad (\vec{n}, \vec{\tau}) = 0.$$

Here $l_{ak}^* = |\vec{x}_k^* - \vec{x}_a^*|$, the point with coordinates $\vec{x}_k$ is the projection of the center of masses of the particle onto the boundary ab.

The value of the tangential force T_c is determined in (6.3) under the assumption of a no-slip condition. In case a law for the friction is given the value T_c determined in (6.3) remains valid when the following inequality is satisfied:

$$|T_c| \leq k|N_c|, \tag{6.4}$$

In case (6.4) is not satisfied, T_c is determined by the formula

$$T_c = k|N_c|\text{sign}(T_c^*), \tag{6.5}$$

where the value T_c^* is given by (6.3). The value of k in (6.4), (6.5) is a friction coefficient. It is evident that on assuming $k = 0$ one obtains a free slip condition on the boundary.

Since the sizes of the particles are final (not infinitely small) the particles interact not only with boundaries but with one another as well. Each particle is characterized by its radius, mass, velocity and coordinate of its center of masses.

Let the line segment l_{ij} connect the centers of i-th and j-th particles (radii r_i and r_j). If the condition

$$l_{ij} < r_i + r_j$$

is satisfied then the particles are in contact. To determine the reaction forces it is necessary to adopt some law for interaction of particles. Using the analogy with the interaction between particles and the boundary one can choose the law of absolutely unelastic impact. Then one has the following sets of formulas:

$$\vec{R}_{l_{ij}} = \frac{\vec{v}_{l_i} - \vec{v}_{l_j}}{\tau m_{ij}}, \quad \vec{R}_{l_{ji}} = -\vec{R}_{l_{ij}}, \quad m_{ij} = \frac{1}{m_i} + \frac{1}{m_j},$$
$$\vec{v}_{l_i} = (\vec{v}_i^*, \vec{l}_{ij})\vec{l}_{ij}, \quad \vec{l}_{ij} = \frac{\vec{x}_j^* - \vec{x}_i^*}{|\vec{x}_j^* - \vec{x}_i^*|}, \tag{6.6}$$

where $\vec{x}_i^*$ – intermediate value for the vector of the i-th particle center; $\vec{v}_{l_i}$ – the projection of the velocity vector on the line connecting the centers of particles; $\vec{l}_{ij}$ – a unit vector along that line.

If there is no friction between the particles then the tangential component of the reaction force vector is zero, and there is no necessity in the corrections of the tangential component of the velocity vector.

If there exists friction given by the law (6.4) then computations are run similar to the case of particle's interaction with a boundary of a rigid body described above.

If the i-th particle interacts with a number of particles then all the vectors of forces are summed up.

If one adopts any other law of particles interactions (that is possible) then it is necessary to define an appropriate function for the kinetic energy.

6.3 Determining the number of fragments within a destructed cell

The number of fragments in destruction of a cell after the dissipation in the cell reaches its critical value cannot be arbitrary. The crack formation is a process that needs energy. Thus the number of fragments obtained in breakup should be found accounting for the balance of the elastic energy accumulated by the material by the time of breakup, and the energy necessary to form all the free surfaces (cracks) bounding fragments:

$$Ek_e = \frac{1}{2}\int_{\Sigma} \gamma ds, \tag{6.7}$$

where Σ is the total area of the free surfaces originating within the cell, γ – energy necessary for breach square unit formation, E – elastic energy accumulated within the cell, k_e – coefficient of elastic energy transformation. The equation (6.7) still leaves some degrees of freedom for determining the number and masses of particles. Thus empirical data on particles sizes distributions in breakups should be taken into account.

References

1. Smirnov N.N., Kiselev A.B., Nikitin V.F., Shevtsova V.M. and Yumashev M.V. First Interim Report on SPC 97-4046. – Moscow-Brussels, 1997, 38 p.
2. Smirnov N.N., Kiselev A.B., Nikitin V.F., Shevtsova V.M. and Yumashev M.V. Second Interim Report on SPC 97-4046. – Moscow-Brussels, 1997, 35 p.
3. Kiselev A.B., Kabak N.Ye. Computational grids with inner contact boundaries explicit observation: techniques of creation. – Modeling in Mechanics, 1990, vol. 4, No. 5, pp. 96-110 (in Russian).
4. Kiselev A.B. Numerical modeling of the thin obstacles inclined penetration using 3D problem statement. Mathematical Investigations, – Kishinev, Moldova, Stinica, 1989, issue 108, pp. 19-26 (in Russian).
5. Goulidov A.I., Fomin V.M., Shebalin I.I. Mesh reconstruction algorithm for numerical solving of the impact problems with crack formation. Proceedings of the Seventh Union Conference. – Novosibirsk, 1982, pp. 182-192 (in Russian).
6. Goulidov A.I., Shabalin I.I. Numerical modeling of curved separation crack formed at plates impact. Numerical Solutions of Elastic and Plastic Problems. – Proceedings of the Eighth Union Conference. Novosibirsk, 1986, pp. 117-121 (in Russian).
7. Goulidov A.I., Shabalin I.I. Numerical realization of boundary conditions in dynamical contact problems. – Novosibirsk, 1987, 37 p. (in Russian).
8. Goulidov A.I., Fomin V.M. Wilkins method modification for the impact problems. – Novosibirsk, 1980, 23 p. (in Russian).